doi:10.14311/ppt.2025.1.16
Plasma Physics and Technology **12**(1):16–21, 2025

DIELECTRIC RECOVERY OF ELECTRIC ARCS CONFINED BETWEEN PTFE AND PA6.6 WALLS

Pierre Corfdir*, Markus Abplanalp, Patrick Sütterlin

ABB Corporate Research Switzerland, Segelhofstrasse 1K, 5405 Baden-Dättwil, Switzerland

* pierre.corfdir@ch.abb.com

Abstract. Plastic ablation plays a key role in the quenching of arcs in low-voltage switchgear. Here, we compare experimentally the arc quenching capacity of polyamide 6.6 (PA6.6) and polytetrafluoroethylene (PTFE). Using a set-up with a topology close to that of a hybrid breaker, we evaluate the impact of the plastic ablation on the current limitation during arcing as well as on the dielectric recovery after current interruption. Our results, supported with the calculations of the transport properties of plasmas consisting of ablated PA6.6 and PTFE, demonstrate the superiority of PA6.6 for arc quenching in low-voltage applications.

Keywords: electric arc, dielectric recovery, arc quenching, PA6.6, PTFE.

1. Introduction

The ablation of plastics plays an essential role in the interruption of fault currents by low-voltage electromechanical circuit breaker. During the high current phase, energy is transfered from the arc to the plastic housing of the breaker. The plastic walls degrade, and vaporize. The vaporized material enters the plasma and changes its composition. At the same time, the local pressure build-up that results from the plastic wall ablation modifies the gas flow [1, 2]. The combination of these processes leads to an increase in the arc voltage that is built up by the circuit breaker, leading to current limiting, thus reducing the peak let-through current and the let-through energy integral (i^2t) [3] of the fault. A high arc voltage build-up is particularly important for DC applications. While in AC, natural current zero crossings provide a chance to interrupt, current interruption in DC can only be achieved by building a voltage that exceeds the voltage of the grid [4].

The material ablated from so-called arc quenching plastics has an impact not only during the high-current phase, but also during the dielectric recovery phase after current zero crossings [2, 5, 6]. While polyamide 6 and polyamide 6.6 (PA6.6) are normally the plastics of choice for arc quenching in low-voltage switchgear [7], polytetrafluoroethylene (PTFE) has been commonly used in medium and high-voltage applications [6]. In particular, the hydrogen released by the decomposition of polyamides leads to an increase in the thermal conductivity of the vapor, which is favorable to recover sufficient dielectric strength.

The actual trend in low-voltage switchgear for industrial applications is to increase the rated voltage from the usual 690 V [8] towards values up to 1000 V and above [9]. Since the selection of the plastic depends not only on the gasing performance during arcing but also on the dielectric properties, it is questionable whether PA6.6 still offers superior performance for these new applications at relatively high voltage.

Here, we compare the arc quenching properties of PA6.6 and PTFE during the arcing and the dielectric recovery phases. The arc burns in a plastic tube placed between two electrodes made of copper. We show that the arc voltage obtained with PA6.6 is favorable for current limitation. At the same time, the cooling of the post-arc vapor after interruption of the current is faster with PA6.6, leading to a faster dielectric recovery.

2. Experimental details

Figure 1(a) describes the electrical circuit used in our study. A 3-level Buck converter is used to deliver a constant current of 1 kA. The capacitance and the inductance used in each level of the Buck converter are $C = 10$ mF and $L = 0.92$ mH, respectively. For all tests, the charging voltage of the capacitors is 1 kV. In order to provide the desired current, we measure the voltage between the electrodes together as well as the actual current and compute the switching times of insulated gate bipolar transistors (IGBTs) located at each of the three levels of the converter. The switching events of the IGBTs exhibit a 120° phase shift to minimize the current ripple [10].

The test object, displayed in Figs. 1(b,c), consists of two cylindrical electrodes made of copper that face each other and that are separated by 55 mm. The diameter of the electrodes is 10 mm, and their tip exhibits a hemispherical shape with a radius of 5 mm. A plastic tube in PA6.6 or in PTFE is centered on the axis of the two electrodes. The length of the tube is 20 mm. The inner diameter (d) of the tube is equal to 5 or 7.5 mm depending on the tests. The tube is hold in place using parts in glass-fiber reinforced PA6.6. The copper electrodes and the plastic tubes have been replaced after each test. The plastic used for the tubes have been commercially sourced and are without fillers. At the beginning of the test, a

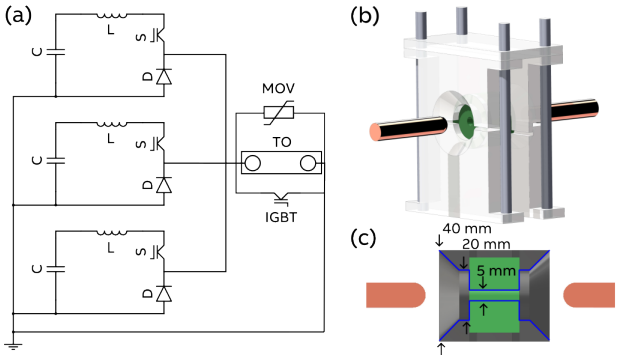

Figure 1. (a) Electric circuit used for our tests. The capacitor banks, the inductance, the IGBT and the body diodes of each level of the Buck converter are labeled as C, L, S and D, respectively. The current is delivered to the test object (TO) mounted in parallel with an IGBT and an MOV. (b) Schematic representation of the test object. The arc burns in a plastic tube (shown in green) between two electrodes in copper (orange). (c) Cross-section view of (b) showing the copper electrodes (orange) the plastic tube (green) and the parts in glass fiber reinforced PA6.6 used to hold the plastic tube (dark grey). The blue lines show the surface exposed to the arc. The diameter at the locations of the arrows is specified directly in the figure.

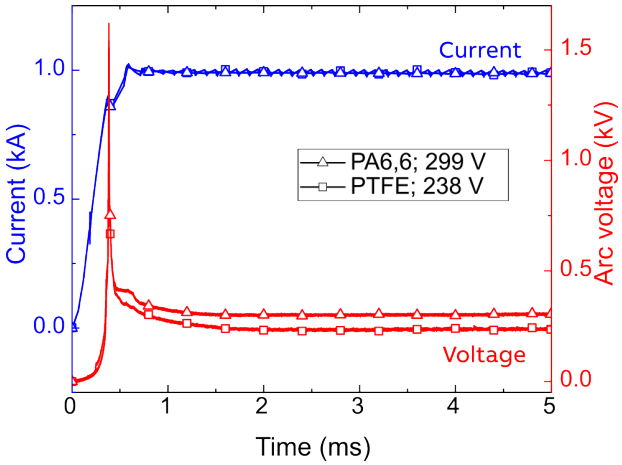

Figure 2. Current (blue, left y-scale) and arc voltage (red, right y-scale) measured during tests on PA6.6 and PTFE tubes with $d = 5$ mm (triangles and squares, respectively). The values in the inset are the mean values of the arc voltage for times between 2.5 and 4.5 ms.

thin copper wire with diameter and length 0.127 mm and 6 cm, respectively, is used to connect the tips of the two electrodes. All experiments have been conducted in ambient air conditions, with no specific measures taken to control the humidity of the testing environment.

The dielectric recovery of switchgear after arcing is normally tested using set-ups that mimic standardized tests (see for instance [11]). Here, we use a different set-up that ressembles that of a hybrid circuit breaker. As shown in Fig. 1(a), an IGBT is mounted in parallel to the test object. When switched on, the current commutes from the test-object to the IGBT. The measurements of the arc voltage and of the current delivered by our Buck converter are used to compute on-the-fly the energy dissipated by the arc. The gate signal that switches on the IGBT is sent once this energy has reached a given threshold, which is set to 1.5 and 3 kJ for all tests in this paper. A metal-oxide varistor (MOV) is also mounted in parallel to the test object and to the IGBT in order to protect the latter from over-voltages. The MOV clamps the voltage to a value of about 5.5 kV.

3. High-current phase

Figure 2 compares the arc voltage build-up measured at 1 kA on the test object with PA6.6 and PTFE tubes with $d = 5$ mm. The current increases from 0 to 1 kA in 0.6 ms. For longer times, the current delivered by our current source is kept nearly constant equal to 1 kA. We highlight the fact that the despite the fluctuations in the arc voltage, the current ripple remains below 30 A. During the first 1 ms of arcing, a sharp voltage spike is detected. This spike is associated with the explosion of the thin copper wire that connects the two electrodes at the beginning of the test [10, 12]. A small difference in peak voltage is seen between PA6.6 and PTFE (1.62 and 1.54 kV, respectively), which we attribute to test-to-test variations in the length and bending of the wire. The peak voltage averaged over 48 shots is 1.45 ± 0.24 and 1.49 ± 0.19 kV for PA6.6 and PTFE. In view of the relatively long arcing times used in this paper, we rule out that these variations have an impact on the results discussed here. In particular, as shown in Fig. 2, the arc voltage after 1 ms of arcing is stable, indicating that the arc is in a quasi steady state.

The mean arc voltage measured using a PA6.6 tube with $d = 5$ mm for arcing times between 2.5 and 4.5 ms is 299 V. Repeating the measurement 18 times yields 299 ± 3 V. The reproducibility of the measurements highlights that the arc in our set-up is stable. which is a result of the confinement of the arc by the walls of the plastic tube. With PTFE tubes with the same d, the mean arc voltage between 2.5 and 4.5 ms and averaged over 18 shots is equal to 238 ± 3 V. The different results obtained with PTFE and PA6.6 indicate that already after 2.5 ms of arcing at 1 kA, some material from the plastic tube was vaporized, modifying the properties of the plasma. As discussed in Ref. [13], the conductance of PTFE gases is larger than that of PA6.6, which is consistent with the arc voltage values observed on Fig. 2.

With increasing d from 5 to 7.5 mm, the average arc voltage measured with PA6.6 and PTFE tubes decreases down to 207 ± 3 and 162 ± 4 V, respectively. We attribute this decrease to the fact that with increasing d, the current density in the tube decreases and the arc voltage is smaller. Since the current is constant in our tests, the decrease in the arc voltage

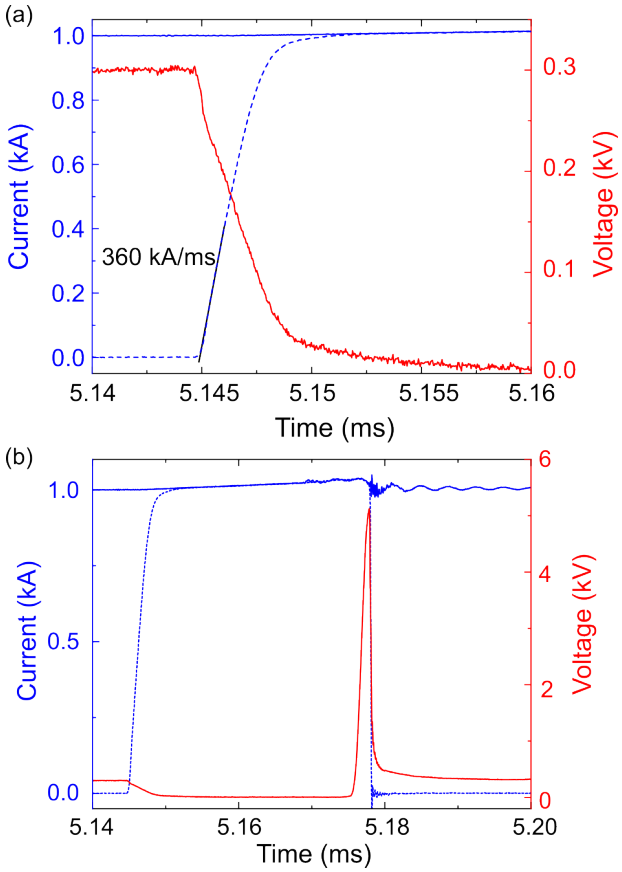

Figure 3. (a) Current delivered by the current source (solid blue line, left y-scale) and voltage (red line, right y-scale) measured during tests on a PA6.6 tube with $d = 5$ mm. The blue dashed line shows the current flowing through the IGBT and the MOV mounted in parallel to the test object. The solid black line is a linear fit to the current through the IGBT and the MOV, which yields a current increase rate of 360 kA/ms. (b) Same as (a) with a larger time window.

leads to a reduction in the energy dissipated by the arc, in the energy transfered from the plasma to the wall, and in the plastic ablation. The pressure build-up is reduced, making the decrease in the arc voltage with increasing d even larger.

4. Current interruption

The interruption of the arc is achieved by switching on the IGBT mounted in parallel to the test object [Fig. 1(a)]. The IGBT is switched on once the energy dissipated by the arc has reached a threshold value of 1.5 kJ. This energy is given by $\int i_{\mathrm{arc}} u_{\mathrm{arc}} \mathrm{d}t$, with i_{arc} and u_{arc} the current and the arc voltage, respectively, and is computed on the fly. A typical current interruption process is shown in Fig. 3(a) for a PA6.6 tube with $d = 5$ mm. The IGBT is switched on once the dissipated arc energy is equal to 1.5 kJ, which occurs after 5.145 ms arcing time. The current in the IGBT (i) rises rapidly and reaches already 900 A after 3 µs. The full current is commuted from the arc after 7 µs. At the same time, the voltage rapidly drops down to the on-state voltage of the IGBT (a few V).

The time needed to commute the current from the test object to the IGBT depends on the arc voltage and on the inductance of the loop formed by our test object and the IGBT (L_{TO}). Once the IGBT is switched on, i is given by:

$$i = \frac{u_{\mathrm{arc}}}{R_{\mathrm{TO}}} \left(1 - \exp\left(-\frac{R_{\mathrm{TO}}}{L_{\mathrm{TO}}} t\right)\right) \qquad (1)$$

with R_{TO} the resistance of the loop formed by our test object and the IGBT. The initial rise of i is nearly linear with a slope equal to $u_{\mathrm{arc}}/L_{\mathrm{TO}}$. As depicted in Fig. 3(a), this slope is equal to 360 kA/ms, which yields $L_{\mathrm{TO}} = 0.83$ µH.

When repeating the test with PTFE tubes with $d = 5$ mm, the initial slope of the current commutation to the IGBT is 290 kA/ms. The value of L_{TO} does not depend on the material used for the tube (it depends only on the length and shape of the current loop between formed by the test object and the IGBT). Therefore, the decrease in current commutation rate seen when going from PA6.6 to PTFE correlates well with the observed decrease in arc voltage from 299 to 238 V discussed in Section 3.

5. Dielectric recovery

After a given time, the IGBT is again switched off and the voltage between the two copper electrodes increases again. Figure 3(b) shows the evolution of the voltage measured for the same test as in Fig. 3(a). In this test, the time delay between the switch-on and the switch-off of the IGBT is $\Delta t = 30$ µs. As shown in Fig. 3(b), breakdown between the copper electrodes occurs when the voltage reaches a peak value of $U_{\mathrm{b}} = 5.18$ kV. After the breakdown, the voltage rapidly decreases down to a value close to the arc voltage in Fig. 2, and the current commutes back to the arcing branch. Note that the oscillations in the total current starting from 5.17 ms in Fig. 3(b) are related to the difficulty for our set-up to regulate the current during the 0.2 ms after the voltage spike. We also emphasize the fact that if the voltage exceeds the clamping voltage of the MOV, the current commutes from the IGBT to the MOV. In other words, with our set-up, we can only probe U_{b} values up to 5.5 kV.

We show in Fig. 4(a) the evolution of U_{b} with respect to Δt for PA6.6 and PTFE tubes with $d = 5$ mm. For all tests, the current is interrupted when an arc energy of 1.5 kJ is reached. For PA6.6, U_{b} increases from 1.95 to 5.2 kV with increasing Δt from 10 to 25 µs. The increase in U_{b} is the fastest for Δt between 10 and 15 µs and slows down for longer times. For Δt larger than 30 µs, the breakdown voltage exceeds the clamping voltage of the MOV and therefore cannot be measured. With PTFE, the increase in U_{b} is much slower: U_{b} reaches 4.4 kV only with $\Delta t = 50$ µs.

We rule out that the slower dielectric recovery for PTFE could be caused by the slower current commutation for this material. As discussed in Section 4,

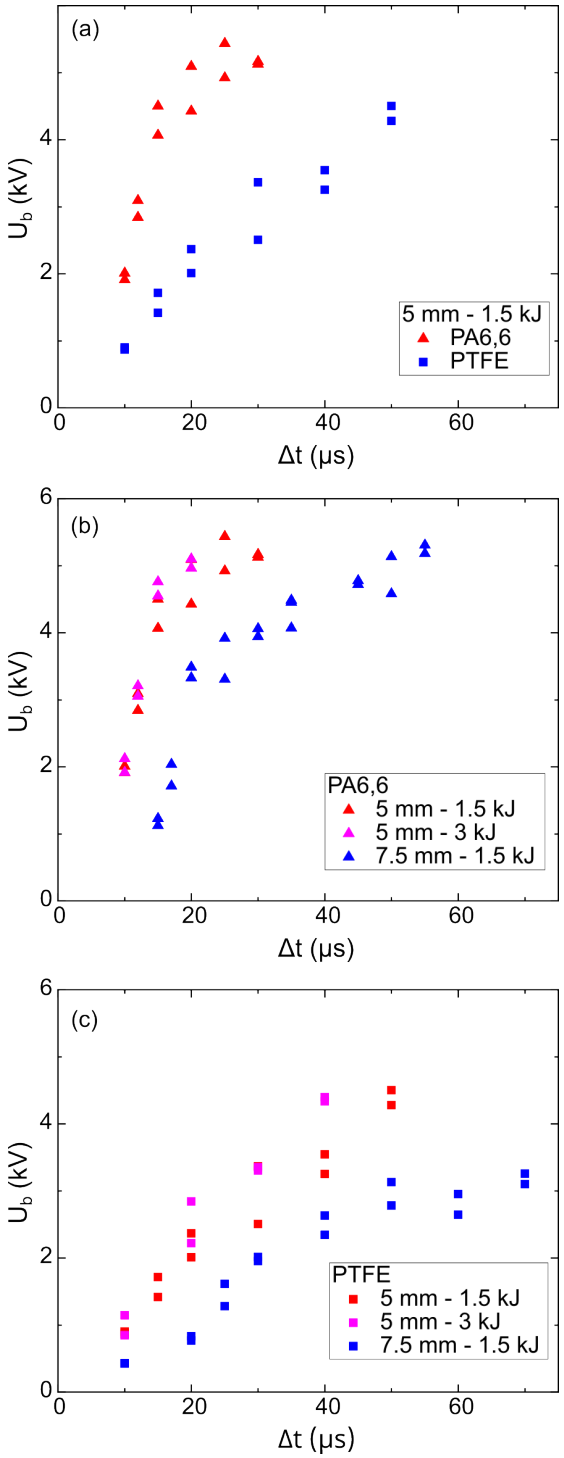

Figure 4. U_b as a function of Δt. (a) PA6.6 and PTFE tubes with $d = 5$ mm after 1.5 kJ arcing event (triangles and squares, respectively). Panels (b) and (c) show results obtained with PA6.6 and PTFE tubes, respectively.

the arc voltage for PTFE during the arcing phase is $\sim 0.8\times$ the one measured with PA66 tubes. As a result, the current commutation with PTFE tubes is completed after 9 µs. This 2 µs delay cannot explain the differences in dielectric recovery seen in Fig. 4.

Additional tests on tubes with $d = 7.5$ mm and with arc energy at interruption equal to 3 kJ have been performed. The results are shown in Figs. 4(b) and 4(c) for PA6.6 and PTFE tubes, respectively. For both materials, the dielectric recovery seen after a 3 kJ arc energy is comparable to that after 1.5 kJ. For all tests on PA6.6, a transition from a fast to a slow increase in U_b is seen for Δt between 15 and 20 µs. For PTFE, this transition is visible for $\Delta t = 50$ µs for the test with $d = 7.5$ mm. Finally, the larger d, the lower U_b. For instance, as shown in Figs. 4(b) for PA6.6, U_b with $\Delta t = 30$ µs decreases from 5.1 to 4.0 kV when d increases from 5 to 7.5 mm.

6. Discussion

The breakdown voltage of the post-arc vapor between the two copper electrodes depends on the pressure, the temperature [14–16] and the composition [17, 18]. These three parameters depend on both the arcing stage (pressure and temperature build-up, change in the plasma composition by vaporization of electrode and plastic tube material) and the cooling stage (temperature decrease and pressure equilibration, electron-ion recombination, formation of small molecules [18, 19], post-arc ablation of the plastic [20]).

The dielectric recovery rate in Figs. 4(b,c) does not depend substantially on the energy of the arcing event. This result confirms that after a few ms of arcing the arc is in a quasi-steady state in terms of temperature, pressure and composition (Section 3). In addition, for a given Δt, U_b decreases with increasing d from 5 to 7.5 mm [Figs. 4(b,c)]. This result agrees well with the fact that with increasing d, the pressure build-up decreases (Section 3), leading to a reduction in the dielectric strength.

We attribute the abprut transition from a fast to a slow increase in U_b with increasing time (Fig. 4) to a change from a fast to a slow cooling down of the post-arc vapor. A two-regime cooling has been already reported by [18] for PA6.6 and and has been ascribed to the formation of small molecules. To further compare the cooling of PA6.6 and PTFE, we have thus computed the thermal conductivity of these gases at 1 bar. Our results are displayed in Fig. 5(a). The results are in good agreement with the results published in [18] and [21] for PA6.6 and PTFE, respectively. Both gases exhibit pronounced thermal conductivity peaks near 3.8 and 3.5 kK, respectively, which we associate with the formation of H_2 and C_2 for PA6.6 and of CF and C_2 for PTFE. The formation of small molecules is not only associated with peaks in the thermal conductivity, but also in the specific heat capacity. Therefore, the cooling is rapid until the dissociation peak is reached and much slower afterwards [18]. Accordingly, the dielectric recovery is fast during the first regime of the cooling, and much slower once the the small molecules have formed, which is consistent with the trends seen in Fig. 4 for PA6.6 and PTFE.

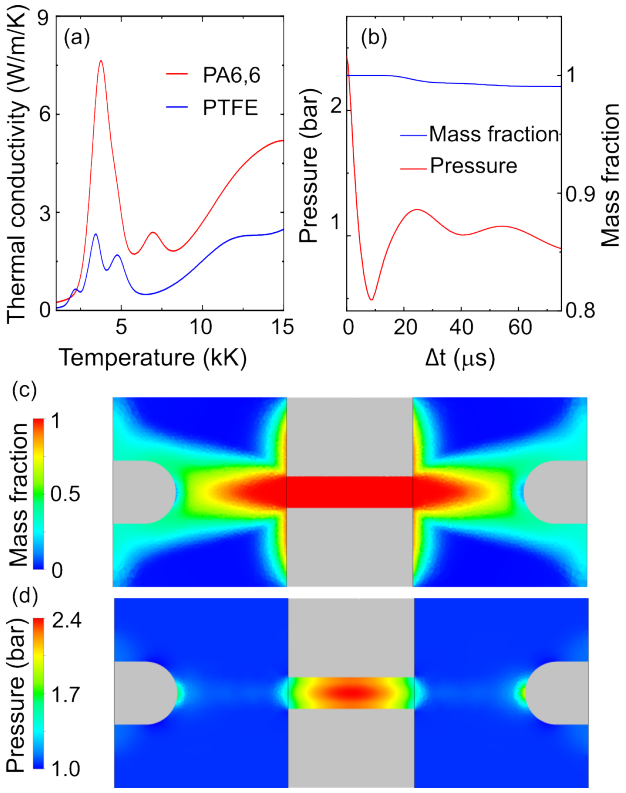

Figure 5. (a) Thermal conductivity of PA6.6 and PTFE plasmas (red and blue lines, respectively) at 1 bar as a function of the temperature. (b) Simulated time-dependence of the pressure (red) and of the mass fraction in vaporized PA6.6 (blue) at the center of a PA6.6 tube after 5 ms arcing at 1 kA. (c). Mass fraction of vaporized PA6.6 after 5 ms of arcing at 1 kA in the symmetry plane of the test object. (d) Same as (c) for the pressure. The mass fraction of vaporized PA6.6 and the pressure in (c) and (d), respectively, are color coded according to the color scales at the left.

The thermal conductivity peaks in Fig. 5(a) are seen in the 3.5–3.8 kK temperature range for both PTFE and PA6.6 gases. Therefore, we expect the temperature of the PA6.6 and PTFE post-arc vapors to be comparable at the transition point between the rapid and the slow cooldown regimes. Since the thermal conductivity peak for the PA6.6 post-arc vapor is about 2.5 times larger than that of PTFE, this transition point is reached more rapidly with PA6.6. This result is consistent with the obervation that, with $d = 7.5$ mm the transition point for PA6.6 and PTFE is reached after 20 and 40 µs, respectively. It is interesting to also note that the time needed to reach the transition point from fast to slow cooling in our work (15–20 µs) is comparable to that reported in [18] for a wall-stabilized arc (20 µs). This finding suggests that the dielectric recovery during the first cooling regime is essentially controlled by the post-arc vapor inside the tube.

Finally, we would like to comment on the fact that U_b for PA6.6 at the transition point is larger than for PTFE [see data with $d = 7.5$ mm in Figs. 4(b) and 4(c), respectively]. Since at the transition point, the temperature of the PTFE and PA6.6 post-arc vapors are comparable, we attribute this difference to a higher pressure in the tube at the transition point for PA6.6 than for PTFE. A lower pressure could indeed be expected for PTFE, seems natural since the transition point for this material is reached ~ 20 µs later than for PA6.6.

To test this idea, we have carried out magneto-hydro-dynamic simulations performed with the tool described in [22]. The results are shown in Figs. 5(b-d) for PA6.6. Figures 5(b) and 5(c) show the pressure and the content in vaporized PA6.6 of the plasma after arcing 1 kA and after an arcing time of 5 ms. This time is comparable to the time at which current interruption takes place in Fig. 3. As depicted in Fig. 5(b), the plasma in the tube consists only of vaporized PA6.6. To the exception of the arc root regions at the tip of the electrode, the content in vaporized PA6.6 in the region between the tube and the electrodes is above 0.5. Therefore, the properties of the plasma during arcing are essentially given by that of the vaporized plastic.

As shown in Figs. 5(b,d), the pressure in the tube during arcing is above the background pressure, with of a peak value of 2.4 bar at the center of the tube. Figure 5(d) depicts the time-dependence of the pressure at the center of a PA6.6 tube with $d = 5$ mm and after arcing at 1 kA. When the current interruption is initiated ($\Delta t = 0$), the pressure in the tube is 2.4 bar. At 20 µs after current interruption, the mass fraction of the post-arc vapor in vaporized PA6.6 remains above 0.99. The pressure has reached a value of 1.1 bar and only shows small oscillations around the background pressure for longer times: the simulation thus demonstrates that at the transition point, the pressure in the PA6.6 tube has already equilibrated with the ambient. Therefore, we attribute the larger U_b seen for PA6.6 at the transition point to a higher reduced electric field at 1 bar in the 3.5–3.8 kK. As an alternative, the different U_b seen for PA6.6 and PTFE could be linked to other effects not included in the simulation like the post-arc ablation of the plastic [20] as well as the presence in the gas of metal drops, plastic residues and soot.

7. Conclusions

In summary, we have compared the arc quenching properties of PA6.6 and PTFE gases during both the high-current and the dielectric recovery phases. The arc voltage build-up with PA6.6 is higher, which is advantageous in low-voltage applications as it limits both the peak let-through current and the i^2t of the fault. With both PTFE and PA6.6, the temperature decreases rapidly down to 3.5–3.8 kK and goes down much slower afterwards. With PA6.6, this transition point is reached faster. As a result, the dielectric recovery is faster with PA6.6. In view of the dimensions of our test object, the larger breakdown

voltage achieved during this fast cooling regime make us conclude that in low-voltage applications even at relatively high rated voltage, the arc quenching behavior of PA6.6 is superior to that of PTFE. In contrast to low-voltage switchgear, high-voltage breakers are not current limiting. Therefore, the low arc voltage build-up, the dielectric and mechanical properties, and the stability of PTFE make it the material of choice for high-voltage applications.

Acknowledgements

We acknowledge Gabriel Lantz for a careful reading of our manuscript.

References

[1] D. Gonzalez, H. Pursch, and F. Berger. Experimental investigation of the interaction of interrupting arcs and gassing polymer walls. *2011 IEEE 57th Holm Conference on Electrical Contacts (Holm)*, pages 1–8, 2011. doi:10.1109/HOLM.2011.6034774.

[2] H. Taxt, K. N., and M. Runde. Medium-voltage load current interruption in the presence of ablating polymer material. *IEEE Transactions on Power Delivery*, 33(5):2535–2540, 2018. doi:10.1109/TPWRD.2018.2803165.

[3] Low-voltage switchgear and controlgear - part 1: General rules. *IEC Standard 60947-1*, pages 1–577, 2020.

[4] P. Corfdir, J. Kalilainen, P. Sütterlin, and M. Gouron. Mobility of arc roots on copper and steel surfaces at low dc currents. *2024 IEEE 69th Holm Conference on Electrical Contacts (HOLM)*, pages 1–7, 2024. doi:10.1109/HOLM56222.2024.10768320.

[5] E. Jonsson, M. Runde, G. Dominguez, et al. Comparative study of arc-quenching capabilities of different ablation materials. *IEEE Transactions on Power Delivery*, 28(4):2065–2070, 2013. doi:10.1109/TPWRD.2012.2227834.

[6] G. J. Gjendal, E. Jonsson, and M. Runde. Ablation-assisted current interruption in a medium voltage load break switch. *ICEC 2014; The 27th International Conference on Electrical Contacts*, pages 1–6, 2014.

[7] L. Petersson, H. Martini, M. Chiaravalli, et al. Biobased engineering plastics a tool to reduce carbon footprint. *The 6th International Conference on Life Cycle Management in Gothenburg*, pages 1–4, 2013.

[8] Low-voltage switchgear and controlgear - part 2: Circuit-breakers. *IEC Standard 60947-2*, pages 1–565, 2024.

[9] P. Arrighetti, P. Corfdir, T. Ilic, and G. Ghiroldi. From pressure measurements in an external cabinet to pressure inside arcing chamber. *2024 IEEE 69th Holm Conference on Electrical Contacts (HOLM)*, pages 1–5, 2024. doi:10.1109/HOLM56222.2024.10768304.

[10] P. Corfdir, G. Lantz, M. Abplanalp, et al. Stark shift measurement as a temperature diagnostic of Cu-dominated thermal plasmas. *J. Phys. D: Appl. Phys.*, 52(27):275203, 2019. doi:10.1088/1361-6463/ab188e.

[11] H. Taxt, K. Niayesh, E. Jonsson, and M. Runde. Experimental investigation on ablation-assisted current interruption-experimental setup and preliminary results. *28th International Conference on Electric Contacts ICEC2016*, pages 397–401, 2016.

[12] P. Corfdir, T. Delachaux, P. Sütterlin, et al. Thermalization dynamics of metal vapor switching arcs. *23rd Int. Conf. on Gas Disch. and Their Appl.*, pages 28–31, 2023.

[13] Y. D. Okano, Y. Goto, E. Kaneko, and M. Fuchikami. Quenching performance of air arc discharge with polymer insulators. *20th Int. Conf. on Gas Disch. and Their Appl.*, pages 199–202, 2014.

[14] M. Seeger, G. Naidis, A. Steffens, et al. Investigation of the dielectric recovery in synthetic air in a high voltage circuit breaker. *Journal of Physics D: Applied Physics*, 38(11):1795, 2005. doi:10.1088/0022-3727/38/11/020.

[15] H.-J. Jang, Y.-H. Oh, K.-D. Song, and Y.-I. Kim. Prediction of reduced critical electric field strength of hot dry air in the temperature range 300–5000 K at 0.1 MPa for medium-voltage switchgear. *AIP Advances*, 10(4):045103, 2020. doi:10.1063/1.5145146.

[16] M. Seeger, M. Muratovic, P. Lu, et al. Dielectric recovery in high voltage gas circuit breakers using CO2. *23rd Int. Conf. on Gas Disch. and Their Appl.*, pages 164–167, 2023.

[17] T. Rokunohe, Y. Yagihashi, F. Endo, and T. Oomori. Fundamental insulation characteristics of air; N2, CO2, N2/O2, and SF6/N2 mixed gases. *Electrical Engineering in Japan*, 155(3):9–17, 2006. doi:https://doi.org/10.1002/eej.20348.

[18] P. Teulet, J. J. Gonzalez, A. Mercado-Cabrera, et al. One-dimensional hydro-kinetic modelling of the decaying arc in air–pa66–copper mixtures: II. study of the interruption ability. *J. Phys. D: Appl. Phys.*, 42(18):185207, 2009. doi:10.1088/0022-3727/42/18/185207.

[19] Y. Tanaka and T. Iijima. Advancements in modeling chemically non-equilibrium decaying arc plasmas in C-F-O gas mixtures. *2024 7th International Conference on Electric Power Equipment - Switching Technology (ICEPE-ST)*, pages 397–402, 2024. doi:10.1109/ICEPE-ST61894.2024.10792462.

[20] Y. Babou, P. Corfdir, and R.-P. Sütterlin. Experimental assessment of PTFE post-arc ablation. *Plasma Physics and Technology*, 6:148–151, 2019. doi:10.14311/ppt.2019.2.148.

[21] H. Wang, W. Wang, J. D. Yan, et al. Thermodynamic properties and transport coefficients of a two-temperature polytetrafluoroethylene vapor plasma for ablation-controlled discharge applications. *J. Phys. D: Appl. Phys.*, 50(39):395204, 2017. doi:10.1088/1361-6463/aa7d68.

[22] P. Arrighetti, P. Corfdir, and T. Ilic. System level and multiphysics approaches to simulate low voltage circuit breaker interruption. *2023 IEEE 68th Holm Conference on Electrical Contacts (HOLM)*, pages 1–5, 2023. doi:10.1109/HOLM56075.2023.10352272.